Supplementary Information – Controlling the morphologies and dynamics in three-dimensional tissues

Rajsekhar Das[1] and Xin Li[1]

Department of Chemistry, University of Texas at Austin, Austin, Texas 78712, USA

Sumit Sinha[2]

Department of Physics, University of Texas at Austin, Austin, Texas 78712, USA

D. Thirumalai[1,2]

[1]*Department of Chemistry, University of Texas at Austin, Austin, Texas 78712, USA and*

[2]*Department of Physics, University of Texas at Austin, Austin, Texas 78712, USA*

(Dated: June 26, 2025)

We provide a brief the description of the organization of the SI. way it is organized. The structures of the three dimensional (3D) tissue in different states are described in section (I). The relation between the viscosity (η) and the relaxation time, τ_α, is discussed in section (II). In section (III), we discuss the effect of finite size on the dynamics of 3D tissue. We describe the behavior of relaxation processes in liquid and glassy states in section (IV). In section (V) we show that the Free volume theory explains the dynamics of 3D tissues. In section (VI), it is shown the geometric properties of cells, such as cell-cell connectivity, are related to tissue dynamics. In section (VII), we show that self-propulsion is required for the viscosity saturation. In section (VIII), we discuss the methods used to determine the crystalline states of a cell in the tissue. The results for 2D simulations are shown in section (IX). The parameters used in the simulations are listed in section (X).

I. STRUCTURES OF 3D TISSUES

Depending on the values of the cell elasticity (E) and Σ, cell size dispersion, tissue dynamics exhibit the characteristics of liquids, glassy, and viscosity saturation (see Fig. 9 (g) in the main text). Even though these states are dynamically distinct, they exhibit similar disordered structures, as illustrated below. Fig. S1 (a) shows a snapshot of the 3D tissue with polydispersity $\Sigma = 8.5\%$ and $E = E_0$, which corresponds to the VS regime (yellow

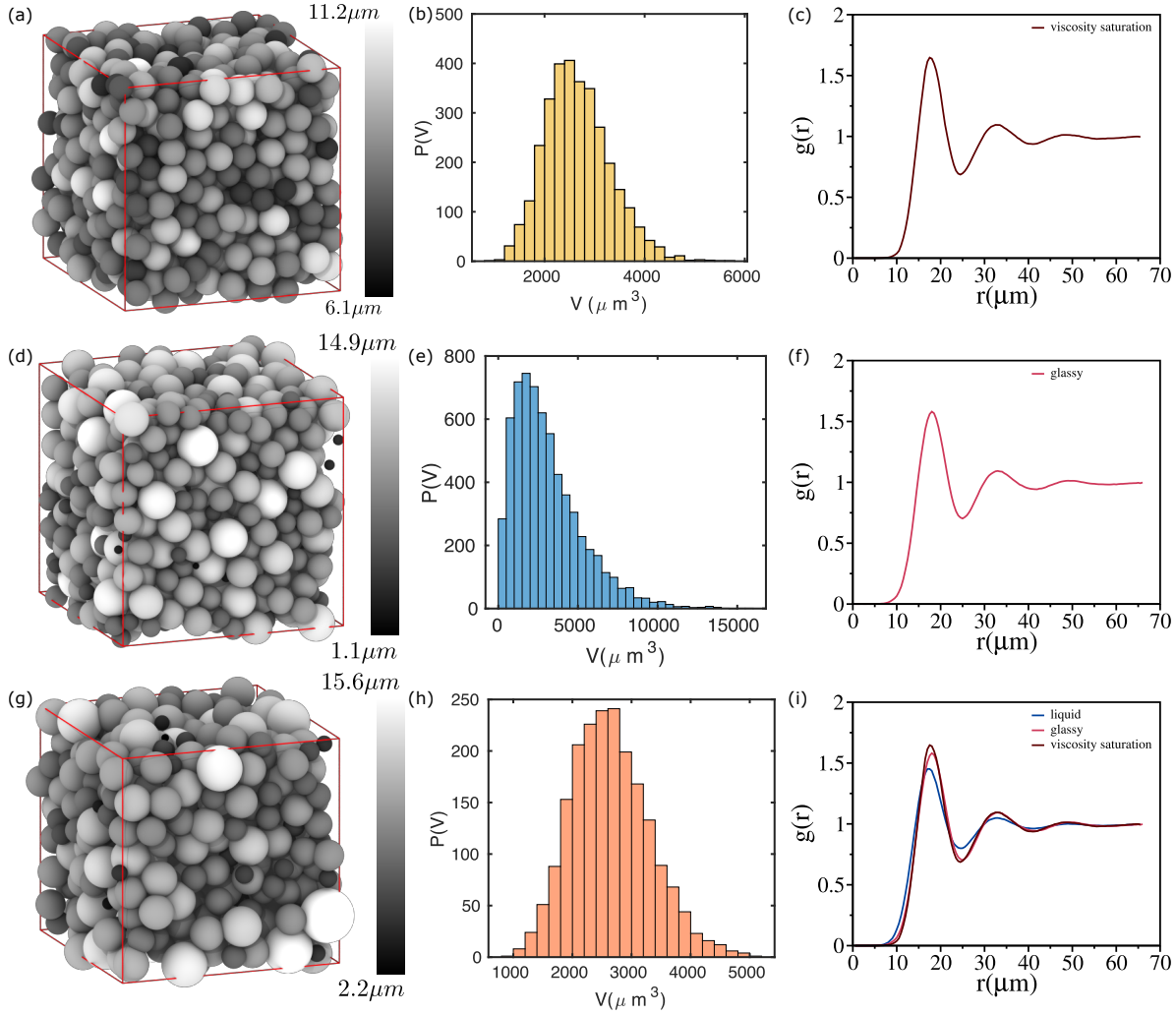

FIG. S1: *Structures of 3D tissues:* Simulation snapshot of a 3D tissue for $E = E_0 = 10^{-3}MPa$, $\Sigma = 8.5\%$ (yellow shaded regime in Fig. 9 (g) in the main text), $\phi = 0.70$ and $N = 800$ (a), for $E = 5E_0$, $\Sigma = 24\%$ (blue shaded regime in Fig. 9 (g) in the main text), $\phi = 0.68$ and $N = 800$ (d) and for $E = 0.2E_0$, $\Sigma = 8.5\%$ (red shaded regime in Fig. 9 (g) in the main text), $\phi = 0.75$ and $N = 500$ (g). Distribution of cell volume for for $E = E_0$, $\Sigma = 8.5\%$, $\phi = 0.70$ and $N = 800$ (b), for for $E = 5E_0$, $\Sigma = 24\%$, $\phi = 0.68$ and $N = 800$ (e) and for $E = 0.2E_0$, $\Sigma = 8.5\%$, $\phi = 0.75$ $N = 250$ (h). Pair correlation function, $g(r)$ as a function of r at $\phi = 0.70$ with $\Sigma = 8.5\%$ and $N = 500$ for $E = E_0$ (c), for $E = 3.0E_0$ (f) and for $E = 0.2E_0$ (i) (blue curve). (i) Comparison of $g(r)$ for VS, glassy and liquid states.

shaded regime in Fig. 9 (g) in the main text). The tissue exhibits an amorphous liquid like structure. The corresponding distribution of volume is shown in Fig. S1 (b).

We characterized the structure using the pair correlation function,

$$g(r) = \frac{1}{\rho}\left\langle \frac{1}{N}\sum_{i}^{N}\sum_{j\neq i}^{N}\delta\left(r - |\vec{r}_i - \vec{r}_j|\right)\right\rangle \tag{1}$$

where $\rho = \frac{N}{L^3}$ is the number density, δ is the Dirac delta function, $\vec{r}_i$ is the position of the i^{th} cell, and the angular bracket $\langle\rangle$ is an ensemble average. Fig. S1 (c) shows that there is no long-range order in the system. We also show the snapshot in the glassy regime (blue shaded regime in Fig. 9 (g) in the main text) in Fig. S1 (d) and liquid regime (red shaded regime in Fig. 9 (g) in the main text) in Fig. S1 (g) with corresponding volume distribution in Fig. S1 (e) and Fig. S1 (h), respectively. The pair correlation function $g(r)$ for glassy and liquid regimes are shown in Fig. S1 (f) and Fig. S1 (i) (blue curve), respectively. However, as shown in Fig. S1 (i), the peaks in the $g(r)$ for liquids are lower than the glass and the system showing viscosity saturation, suggesting liquids are more disordered.

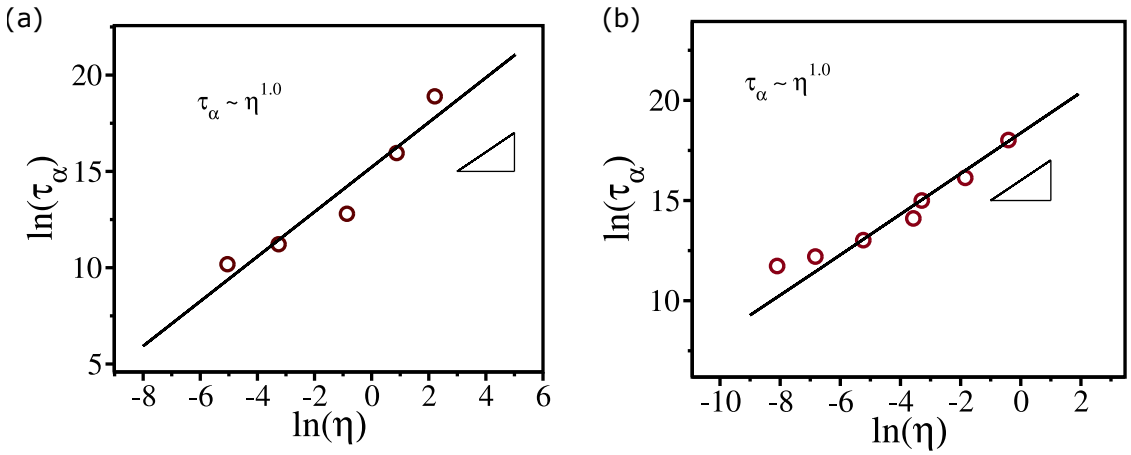

FIG. S2: *Relation between η and τ_α:* (a) Relaxation time, τ_α, as a function of η for $\phi \leq \phi_S$ for the 3D non-confluent tissue with $\Sigma = 8.5\%$ and $E = E_0$ (VS regime – yellow shaded regime in Fig. 9 (g) in the main text). (b) Same as (a) except the results are in 2D with $\Sigma = 24\%$. Small triangles with slope 1 are a guide to the eye.

II. VISCOSITY AND STRUCTURAL RELAXATION TIME ARE LINEARLY RELATED

Because the calculation of η is computationally intensive, in some instances we substituted τ_α as a proxy. This can only be justified if η and τ_α are linearly proportional to each other, which is not always the case in supercooled liquids [1]. For this reason, it is necessary to verify the relation $\eta \sim \tau_\alpha$ in the current cell model. Plots of τ_α as a function of η (for $\phi \leq \phi_S$ – Fig. 2 in the main text) on a log-log scale (Fig. S2 (a) and (b)) show that τ_α and η are proportional to each other both in 3D (Fig. S2 (a)) and 2D (Fig. S2 (b)). Therefore, using τ_α as a proxy for η is justified.

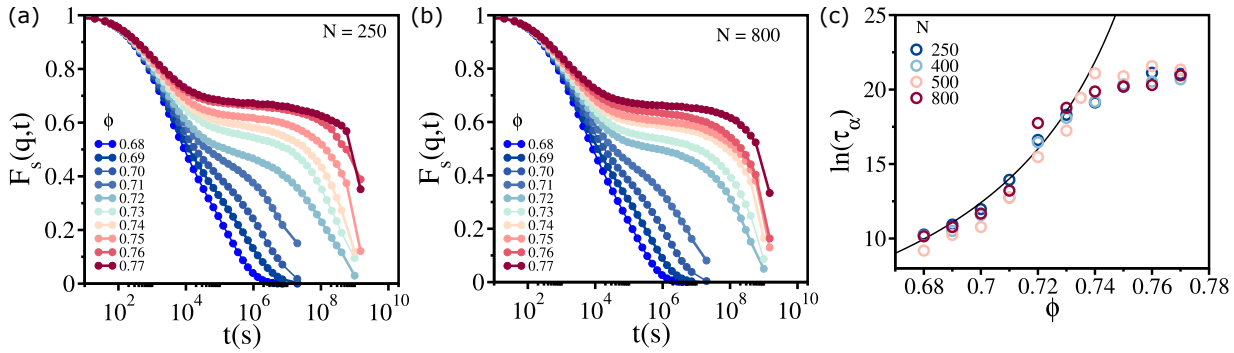

FIG. S3: *Finite system size effects in 3D tissues:* The self-intermediate scattering function, $F_s(q,t)$ (Eqn. (1) in the main text), as a function of t for $0.68 \leq \phi \leq 0.77$ with $E = E_0$ and $\Sigma = 8.5\%$. The value of $N = 250$ (a) and $N = 800$ (b). Relaxation time τ_α as a function of ϕ for $N = 250, 400, 500$ and 800. The solid line is a fit to the VFT equation (see Eqn. 2.)

III. FINITE SIZE EFFECTS

In the main text, we reported the results for $N = 500$. To assess the effects of the finite system size on tissue dynamics, particularly in the VS regime (yellow shaded regime in Fig. 9 (g) in the main text), we performed simulations using $N = 250, 400$, 500, and 800. The variation in N is not too large because the computations are numerically difficult to carry out for N that is significantly greater than 800. The results for $F_s(q,t)$ are presented in

Fig. S3 (a) and (b) for $N = 250$ and 800 respectively. Fig. S3 (c) shows that τ_α and ϕ_S (~ 0.74) values are independent of N in the simulated range. Because the N values were varied only over a very limited range (for computational reasons), we cannot be certain that the results are truly independent of system size.

IV. SHORT AND LONG RELAXATION TIMES IN LIQUID AND GLASSY PHASES

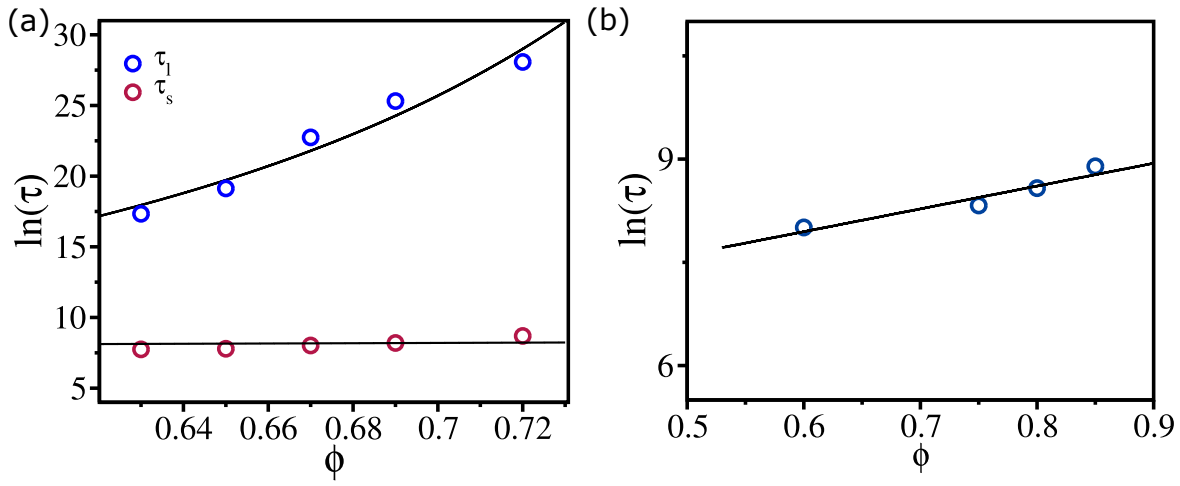

FIG. S4: *Relaxation times as a function of ϕ:* (a) Short (τ_s) and long (τ_l) relaxation times as a function of ϕ calculated using the data Fig. 4 (a) in the main text (glassy dynamics for $\Sigma = 8.5\%$ and $E = 5E_0$). Although τ_l is well fit by the VFT equation (Eqn. (2)), τ_s follow the Arrhenius law, $\tau_s = \tau_0 \exp(A\phi)$. (b) The relaxation time τ, calculated from Fig. 1 (a) main text, as a function of ϕ in the liquid phase ($\Sigma = 8.5\%$ and $E = 0.2E_0$). The increase in τ follows the Arrhenius law $\tau = \tau_0 \exp(A\phi)$ (solid line).

In the liquid phase, the self-intermediate scattering function $F_s(q,t)$ decays in a single step, as shown in Fig. 1 (b) in the main text. The dependence of $F_s(q,t)$ on t is fit by a single stretched exponential function (Fig. 1 (b) in the main text). The estimated relaxation time τ follows the Arrhenius law $\tau = \tau_0 \exp(A\phi)$ (Fig. S4 (b)).

In the glassy state, $F_s(q,t)$ decays in two steps. Initially, there is a fast relaxation, and at long times, there is a slow stretched exponential decay (see Fig. 4 (a) in the main text). We calculated the short and long relaxation times τ_s and τ_l using the fitting procedure described

in the main text. Fig. S4 (a) shows that τ_l grows as ϕ increases, and well fit by the VFT law given by

$$\tau_\alpha = \tau_0 \exp\left[\frac{D}{\phi_0/\phi - 1}\right], \tag{2}$$

where D is a material dependent parameter, and ϕ_0 is the cell packing fraction at which τ_α is expected to diverge. In contrast, the dependence of τ_s is best described by $\tau_s = \tau_0 \exp(A\phi)$ (Fig. S4 (b)).

V. FREE VOLUME THEORY

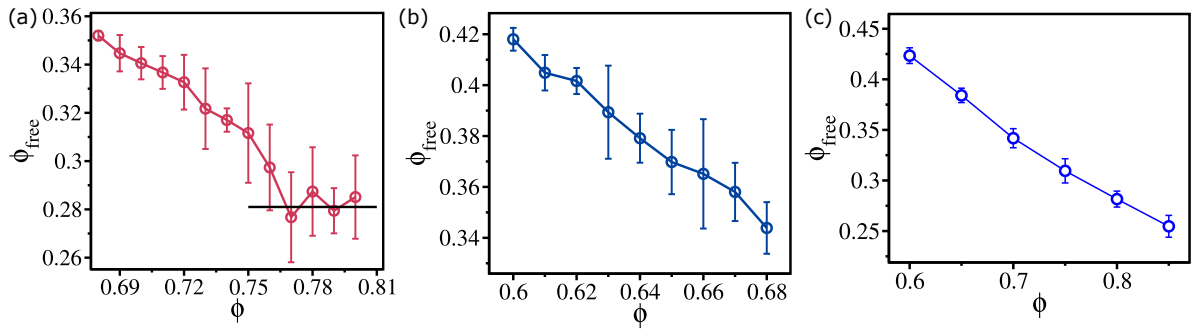

FIG. S5: *Free volume in 3D tissues:* (a) Free volume ϕ_{free} (Eqn. (3)) for $E = 0.8E_0$ and $\Sigma = 8.5\%$ (VS regime) as a function of ϕ. (b) Same as (a), except it is for $E = 5E_0$ (glassy regime). (c) Same as (a) and (b) but for $E = 0.2E_0$ (liquid phase).

In a previous study [2], using 2D simulations, we showed that the saturation of the effective viscosity at high area fraction could be understood using the free volume theory [3–6]. In order to determine whether the free volume ($\phi_{\mathbf{free}}$) theory explains both the monotonic growth of η_{eff} in the glass-like state as well as the saturation in the VS regime in 3D tissues, we calculated the dependence of free volume fraction $\phi_{\mathbf{free}}$ (defined below) as a function of ϕ. We estimated $\phi_{\mathbf{free}}$ by first calculating the Voronoi cell volume (V) for all the cells at each snapshot. We define $V_{\text{free},i} = V - 4/3\pi R_i^3$ where R_i is the radius of the i^{th} cell. The value of V_{free} could be negative if the overlap between the neighboring cells is substantial; V_{free} is positive only when the Voronoi volume is greater than the actual cell volume. The positive value of V_{free} is an estimate for the available free volume. The availability of free volume for a cell facilitates the mobility of jammed cells by cooperative motion of the neighboring cells.

The effective free volume fraction $\phi_{\mathbf{free}}$ is,

$$\phi_{\text{free}} = \frac{\sum_{j=1}^{N_t} \sum_{i=1}^{N_p} V^j_{\text{free}_{+,i}}}{N_t V_{\text{box}}}, \tag{3}$$

where N_p is the number of cells for which the associated free volume is positive, $V^j_{\text{free}+}$ is the value in j^{th} snapshot, N_t is the total number of snapshots, and V_{box} is the volume of the simulation box. The effective free volume of certain cells with substantial overlap would have negative values of V_{free}. In such cases, the Voronoi volume of the cell would be less than the actual cell volume. For our purpose, the free volume is the positive value of V_{free}. Only if V_{free} is greater than zero, there is available space for the cells to move.

We find that $\phi_{\mathbf{free}}$ saturates when $\phi > \phi_S$ in the VS regime (Fig. S5 (a)) whereas it monotonically decreases in the glass-like state (Fig. S5 (b)) and liquid (Fig. S5 (c)). Interestingly, $\phi_{\mathbf{free}}$ decreases almost linearly as ϕ increases in the liquid phase, which means that even in the dense ergodic tissue, the cells can be jammed. The results show that the notion of free volume provides a unified explanation for both the monotonic growth of η_{eff} in the glass-like state and saturation in the VS.

VI. VISCOSITY DEPENDS ON CELL CONNECTIVITY

It is surprising that the striking experimental observation that saturation of viscosity at high ϕ in zebrafish blastoderm tissue [7] could be quantitatively explained using cell-cell contact topology, a purely geometric measure, which was estimated using the average connectivity between cells, $\langle C \rangle$. It was also shown that cell packing fraction was linearly related to $\langle C \rangle$. Two-dimensional simulations [2] showed that the average coordination number $\langle N_c \rangle$, which is equivalent to $\langle C \rangle$ and $\langle C \rangle$ and $\langle N_c \rangle$, was linearly related to ϕ. More importantly, we established [2] that η_{eff} is determined by $\langle N_c \rangle$, which was first pointed out in the elsewhere [7]. We tested if these findings also hold in 3D tissues.

Let us define the coordination number, $\langle N_c \rangle$, as the number of cells that are in contact with a given cell. Two cells, with indices i and j, are deemed to be in contact if $h_{ij} = R_i + R_j - r_{ij} > 0$. At each value of ϕ, we calculated N_c for all the cells and corresponding distribution $P(N_c)$ (Fig. S6 (a), (b) & (c)). The distributions $P(N_c)$ are well fit by a Gaussian function $A \exp\left[-(\frac{x-\langle x \rangle}{\sigma})^2\right]$, where $\langle x \rangle$ is the mean and σ is the dispersion. The mean $\langle N_c \rangle$ calculated from the distribution varies linearly with ϕ (Fig. S6 (d)), which implies

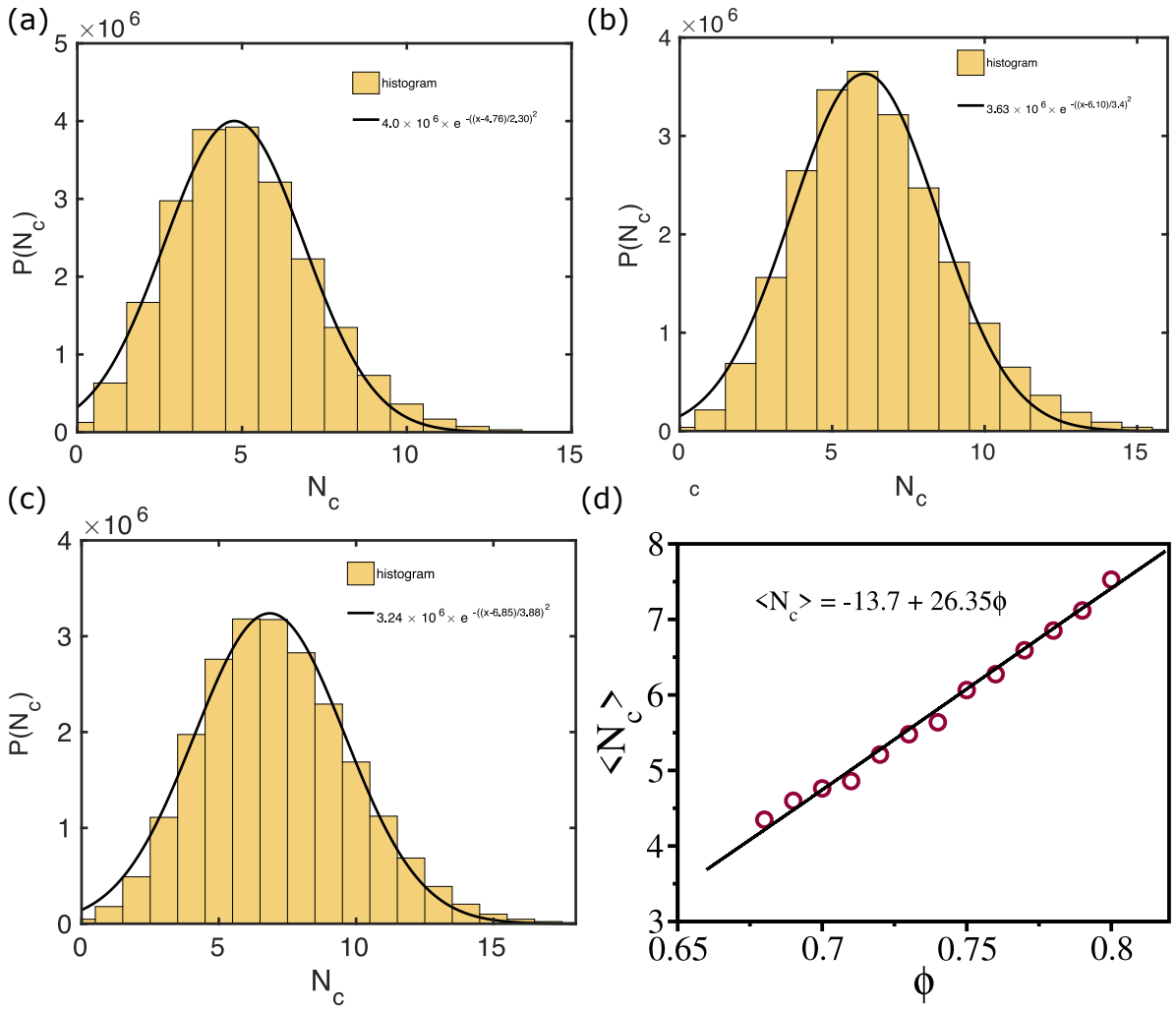

FIG. S6: *Mean coordination number and cell packing fraction:* $P(N_c)$ at $E = 0.8E_0$ and $\Sigma \sim 8.5\%$ for $\phi = 0.70$ (a), for $\phi = 0.75$ (b) and for $\phi = 0.78$ (c). The solid lines are the Gaussian fits. (d) The mean coordination number $\langle N_c \rangle$ as a function of ϕ. The solid line is a linear fit to the data.

that $\langle N_c \rangle \simeq \langle C \rangle$.

Next, we calculated the average connectivity $\langle C \rangle$. We defined each cell as a node and the line connecting the two nodes as an edge (see Fig. S7 (a)). If a snapshot has n nodes and m edges then, $\langle C \rangle = \frac{2m}{n}$. Fig. S7 (b) shows that $\langle C \rangle$ is linearly related to ϕ. Strikingly, $\langle C \rangle$ and $\langle N_c \rangle$ has similar values and also are linearly related (Fig. S7 (c)). Finally, η_{eff} grows as function of $\langle N_c \rangle$ (Fig. S7 (d)), which shows that η_{eff} mirrors the dependence $\langle N_c \rangle$ on ϕ. These results show that even in 3D the complex cell contact network determines the viscosity, which is surprising but supports the finding in the previous study [7].

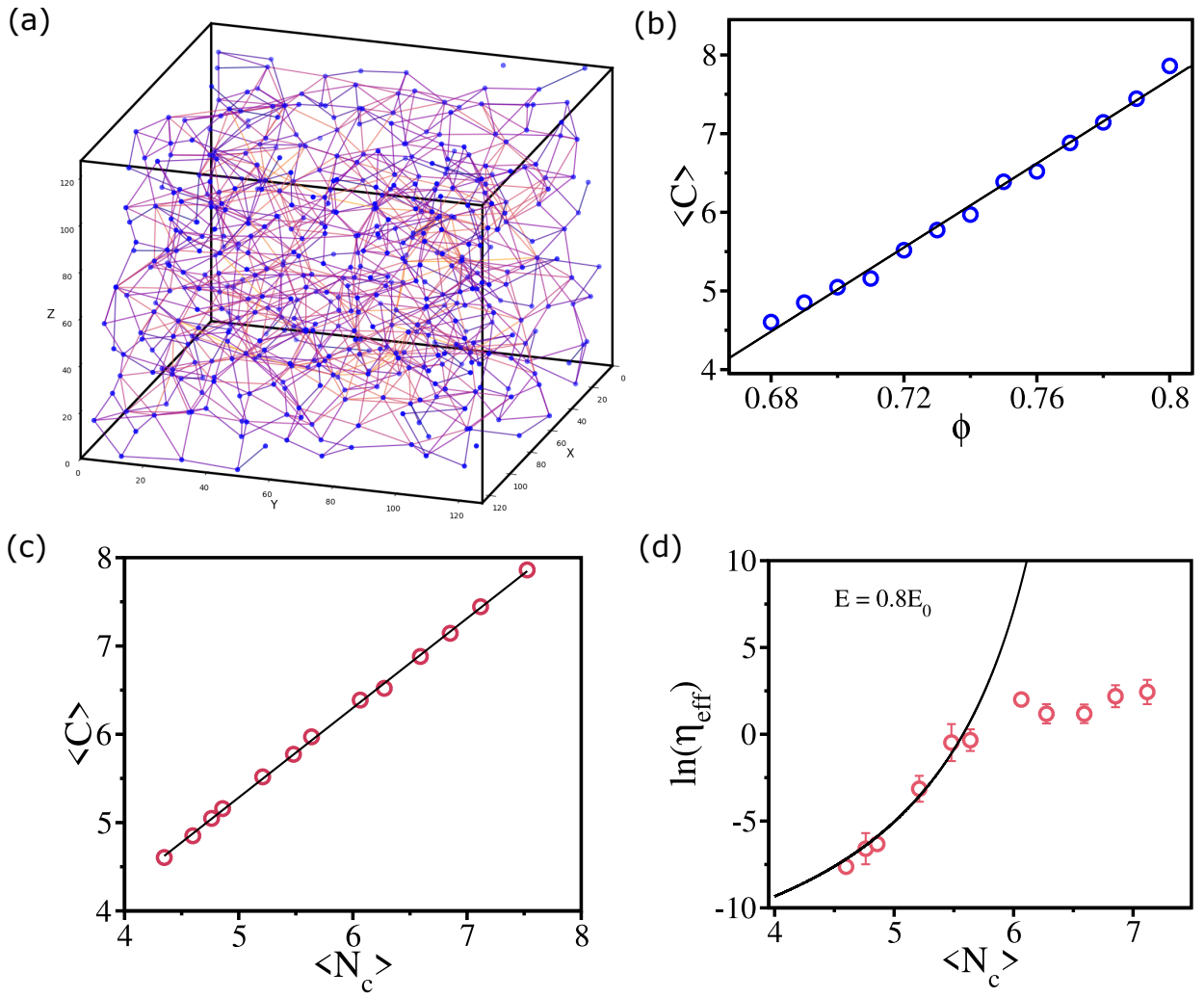

FIG. S7: *Viscosity and cell contact network topology are related:* (a) Sample connectivity map at $\phi = 0.75$, $E = E_0$ and $\Sigma = 8.5\%$, corresponding to the VS regime (Fig. 9 (g) in the main text). The blue dots are the cell centers (node) and lines are the edges. (b) Cell connectivity $\langle C \rangle$ is a linear function of ϕ. (c) $\langle C \rangle$ as a function of network coordination number, $\langle N_c \rangle$. The solid line is a linear fit to the data. (d) Logarithm of the effective viscosity η_{eff} as a function of $\langle N_c \rangle$. The solid line is the VFT fit (Eqn. (2)) to the η_{eff} data.

VII. ON THE IMPORTANCE OF SELF-PROPULSION

In the main text, we showed that the minimal model that reproduces the saturation in viscosity should include self-propulsion (Eqn. 12 in the main text). Depending on the parameters (Σ and E), the tissues exhibit a range of behavior, including the increase in

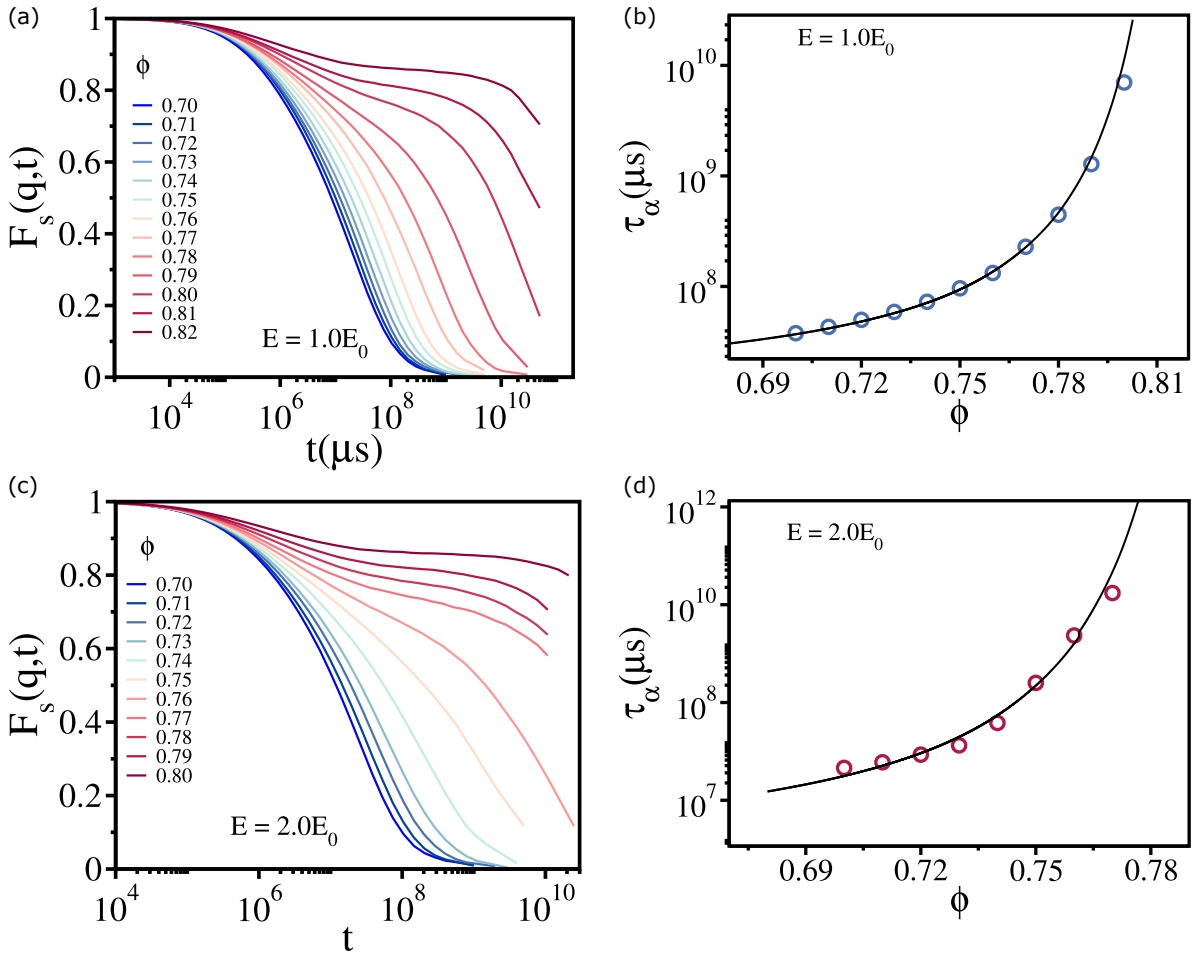

FIG. S8: *Glassy state in 3D tissues:* (a) $F_s(q,t)$ as a function of t for $0.70 \leq \phi \leq 0.82$. (b) Relaxation time τ_α as a function ϕ. The solid line is the VFT fit (Eqn. 2) to the data. We set $\Sigma = 24.8\%$, $E = E_0 = 0.001$ MPa and temperature $T = 300K$. (c) Same as (a) except it is for $E = 2.0E_0$ and $\Sigma = 8.5\%$. (d) Same as (b) except for the parameters values, shown in (c).

viscosity like in glasses below a critical volume fraction followed by a saturation (the VS regime – Fig. 9 (g) yellow shaded regime in the main text). It is natural to wonder if the VS behavior could be reproduced using simulations performed at a fixed temperature. To explore if the results could be explained by merely varying the temperature, we performed Brownian dynamics simulations using the cell model by integrating the equations of motion,

$$\dot{\vec{r_i}} = \frac{\vec{F_i}}{\gamma_i} + \sqrt{(2k_BT/\gamma_i)}\vec{\zeta_i}(t), \tag{4}$$

where $\gamma_i = 6\pi\eta R_i$ with R_i the radius of cell i, $\vec{r_i}(t)$ is the position of a cell at time t; $\vec{\zeta_i}$ is the random noise that satisfies $\langle\vec{\zeta_i}(t)\rangle = 0$ and $\langle\vec{\zeta_i}(t)\vec{\zeta_j}(t')\rangle = 6\frac{k_BT}{\gamma}\delta_{ij}\delta(t-t')$, where δ_{ij} and

$\delta(t-t')$ are Kronecker δ and Dirac δ function. Note that unlike the equation of motion used in the main text, Eqn. 4 obeys the fluctuation-dissipation theorem (FDT). The simulations

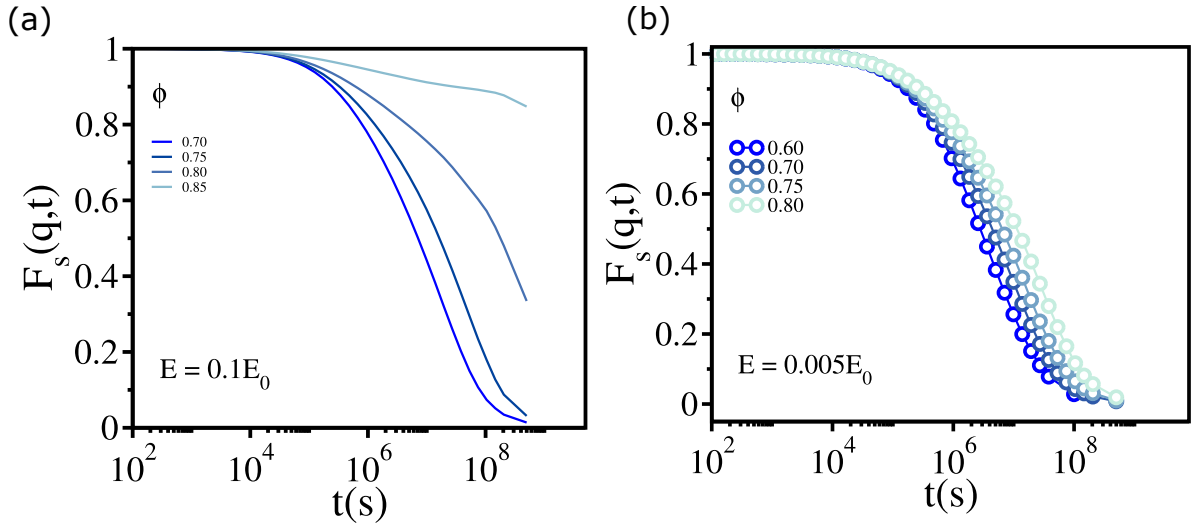

FIG. S9: *Liquid state in 3D tissues using FDT:* (a) $F_s(q,t)$ as a function of t for $0.70 \leq \phi \leq 0.85$ with $E = 0.1E_0$. (b) Same as (a) but for $E = 0.005E_0$. $\Sigma = 8.5\%$ in both (a) and (b).

were performed using $\eta = 5 \times 10^{-6}\ kg/(\mu m \cdot s)$, $E = 10^{-3}$ MPa and $\delta t = 10\ \mu s$. For the parameters used in the temperature simulations, we find that the tissue exhibits only the characteristics of glassy dynamics without signs of saturation in τ_α, which is found in Fig. 2 (b), Fig. 2 (d) and Fig. 2 (e) in the main text. The decay $F_s(q,t)$ occurs in two steps, at most of the values of ϕ, with a clear plateau, especially at high ϕ (Fig. S8 (a)). The calculated relaxation time τ_α follows the VFT law (Fig. S8 (b)). We also performed simulations with $E = 2.0E_0$ and $\Sigma = 8.5\%$ and found a similar result (Fig. S8 (c) and (d)).

The absence of VS under conditions that satisfy the FDT does not prove that saturation of τ_α cannot arise using Eqn. (4) if a broader range of cell softness and Σ are explored. However, it is unlikely that the observed VS in the non-equilibrium simulations, with ($0.3 \lesssim E/E_0 \lesssim 2$) and $\Sigma > 8\%$ explored in Fig. 7 in the main text, could be reproduced using the FDT-satisfying Brownian dynamics simulations (Eqn. (4)). We surmise that a balance between self-propulsion, E, and dispersion in cell size is required to recapitulate the VS behavior.

We also tested how the liquid state is affected when the self-propulsion is absent. We found that in the presence of finite temperature and in absence of self-propulsion, we need to simulate much softer cells ($E = 0.005E_0$) to observe the liquid-like behavior (Fig. S9

(b)), which was found for $E = 0.1E_0$ in the presence of self-propulsion. For temperature simulation with $E = 0.1E_0$, we see a glassy behavior (Fig. S9 (a)).

VIII. COMMON NEIGHBOR ANALYSIS FOR IDENTIFYING CRYSTAL STRUCTURES

We used the Common Neighbor Analysis (CNA) [9] method to identify the local atomic structures based on the topology of atomic bonds. In this approach, two atoms are considered bonded if their separation distance is within a predefined cutoff radius (r_{cut}), chosen based on the crystal structure. For the FCC and HCP structures, r_{cut} is set midway between the first and second nearest-neighbor shells, and for BCC structures, it includes both first- and second-nearest neighbors (see Fig. S10 (c) and (d) for illustration). For each bonded pair, a characteristic triplet (n_{cn}, n_b, n_{1cb}) is computed, where n_{cn} represents the number of shared neighbors between two atoms. n_b is the number of bonds between these common neighbors and n_{1cb} is the longest chain of bonds connecting them. The triplets are calculated for a given snapshot and compared with the known values of perfect crystals. For example, the CNA for FCC is (4,2,1), for BCC (6,6,6) for diamond cubic (5,4,3). The CNA method efficiently distinguishes between different crystalline structures.

In a multiphase system an adaptive common neighbor analysis (a-CNA) was chosen to identify the local atomic structure [9]. Unlike conventional CNA, which relies on a fixed global cutoff radius, a-CNA determines an adaptive cutoff radius that is specific to each atom based on the local environment. The method begins by identifying the N_{max} nearest neighbors for each atom and sorting them according to their distances. To assess whether the local environment matches a given reference structure, the first N nearest neighbors required for that structure are selected, and a local cutoff radius is computed as a function of their average bond lengths. For FCC and HCP structures, the local cutoff radius is determined using the first 12 nearest neighbors, while for BCC structures, both first and the second nearest neighbors cells are considered. The calculated values of the triplets (n_{cn}, n_b, n_{1cb}) are compared with the known values for a perfect crystals. The adaptive cutoff improves the classification accuracy in systems with multiple phases or varying local densities by ensuring that each atom is analyzed using a cutoff that best matches the local immediate environment. In Fig. S10 we show a snapshot of simulations with $\Sigma = 0$ and $E = E_0$ that

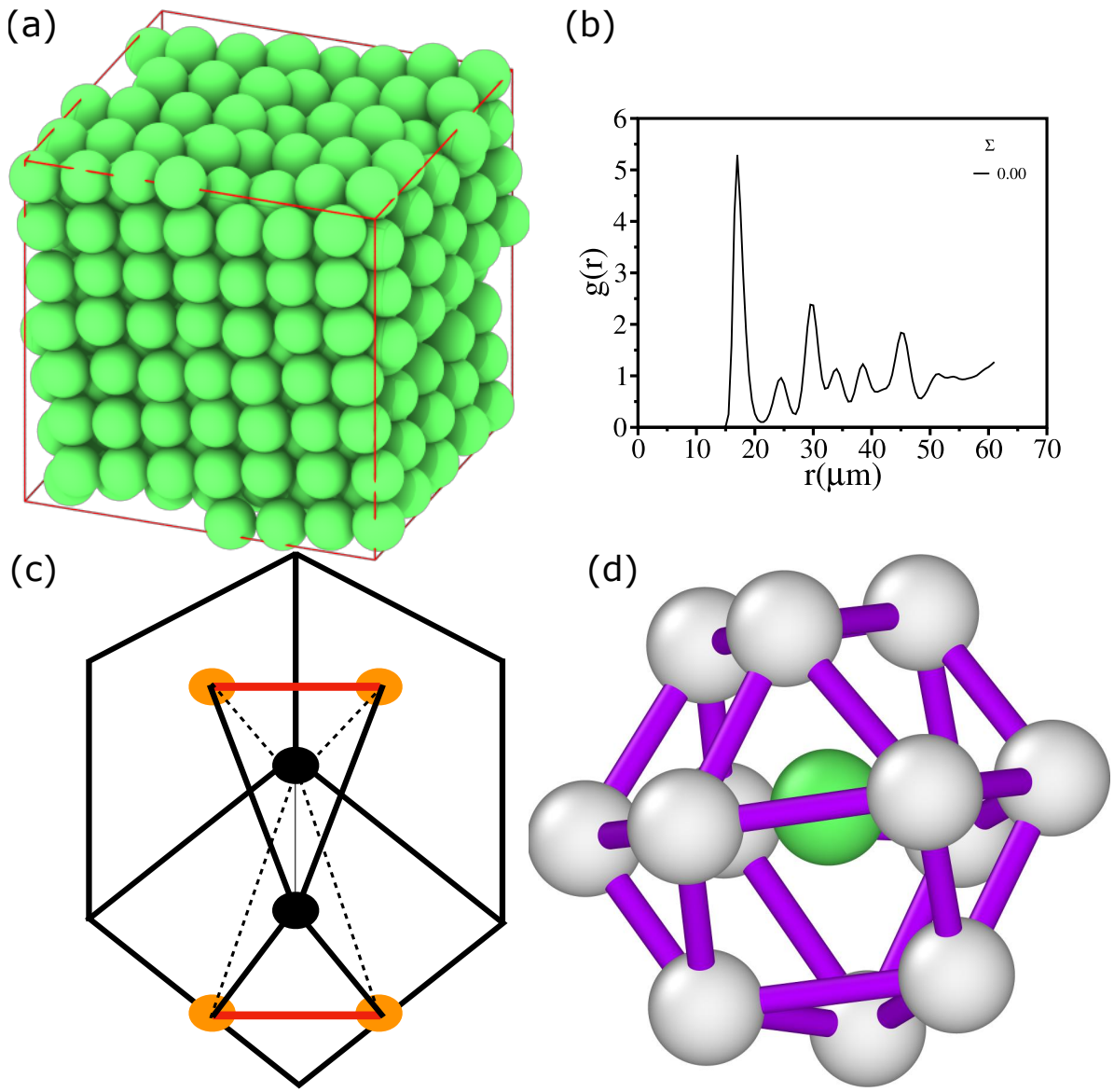

FIG. S10: *Perfect FCC Crystal using a-CNA:* (a) Simulation snapshot for $E = E_0$ with $\Sigma = 0$. The cells are colored green if they match the CNA values for a perfect FCC crystal (4,2,1). (b) The corresponding $g(r)$ as a function of r. (c) Illustration of Common neighbor analysis using three indices (n_{cn}, n_b, n_{1cb}) for a FCC crystal [8]. The bonded atoms in the pair are colored black. The number of neighbors (n_{cn}) common to these atoms is colored yellow. The bonds between the common neighbors (n_b) are colored in red. (d) Example of total 12 common neighbors for an FCC crystal type cell (colored green). The actual cell size is scaled to 60% for a better visualization. $E = E_0$ and $\Sigma = 0$ and $\phi = 0.77$ for (d).

results in the formation of a perfect FCC crystal.

IX. TWO-DIMENSIONAL SIMULATIONS

In the main text, we showed that a 3D non-confluent tissue exhibits the characteristics of a fluid when the $E \lesssim 0.2E_0$, and it exhibits glassy dynamics when $E \gtrsim 3.0E_0$. These characteristics are found provided the cell size dispersion Σ exceeds a critical value (see the diagram of states in Fig. 7 (d) in the main text). Additionally, there is a range of E over which the tissue exhibits viscosity saturation as a function of ϕ. To verify whether a 2D tissue exhibits a similar range of behavior, we performed simulations by varying E at a fixed value of $\Sigma = 24.8\%$, which the estimated previously [2] by analyzing the experimental data [7].

Liquid and glassy behavior: For $E = 0.2E_0$ the decay of $F_s(q,t)$ is nearly independent of ϕ for $0.85 \leq \phi \leq 0.93$ (Fig. S11 (a)), which is reflected in the modest increase in τ_α as a function of ϕ (Fig. S11 (b)). The tissue behaves like an ergodic liquid. On the other hand, at $E = 5E_0$, the tissue exhibits the characteristics of glass-like dynamics. $F_s(q,t)$ decays in two distinct steps with a clear plateau appearing at the intermediate timescales (Fig. S11 (c). The duration of the plateau increases as ϕ increases. At the intermediate timescales the cells get "caged" by their neighbors, which means that the mobility a cell requires movement of a number of other cells. The relaxation time τ_α increases rapidly and is well described by the VFT law (Eqn. (2)) (Fig. S11 (d)).

Viscosity saturation (VS): In the range, $0.8E_0 \leq E \leq 2E_0$, the tissue exhibits the characteristics of viscosity saturation. The relaxation time, as a function of ϕ grows according to the VFT law (Eqn. (2)) when $\phi \leq \phi_S$. When ϕ exceeds ϕ_S, τ_α is independent of ϕ (Fig. S12 (a)). As in the 3D tissues, the ϕ_S value decreases as E increases (Fig. S12 (b). In addition, ϕ_0 decreases (Fig. S12 (c)) and fragility the rate at which τ_α increases with ϕ) increases with E (Fig. S12 (d)). We calculated the kinetic fragility $K = 1/D$ (see Eqn. (2)). As shown in the inset of Fig. S12 (d), it increases by a factor of ~ 2.5 when E changes from $0.8E_0$ to $5E_0$ which suggests as the cells become more deformable, the glass transition should appear at a higher packing fraction than for an equivalent hard sphere system. In synthetic materials the glass transition packing fraction ϕ_g is defined as the packing fraction where viscosity $\sim 10^{13}$ poise or relaxation time goes to ~ 100 s. Following

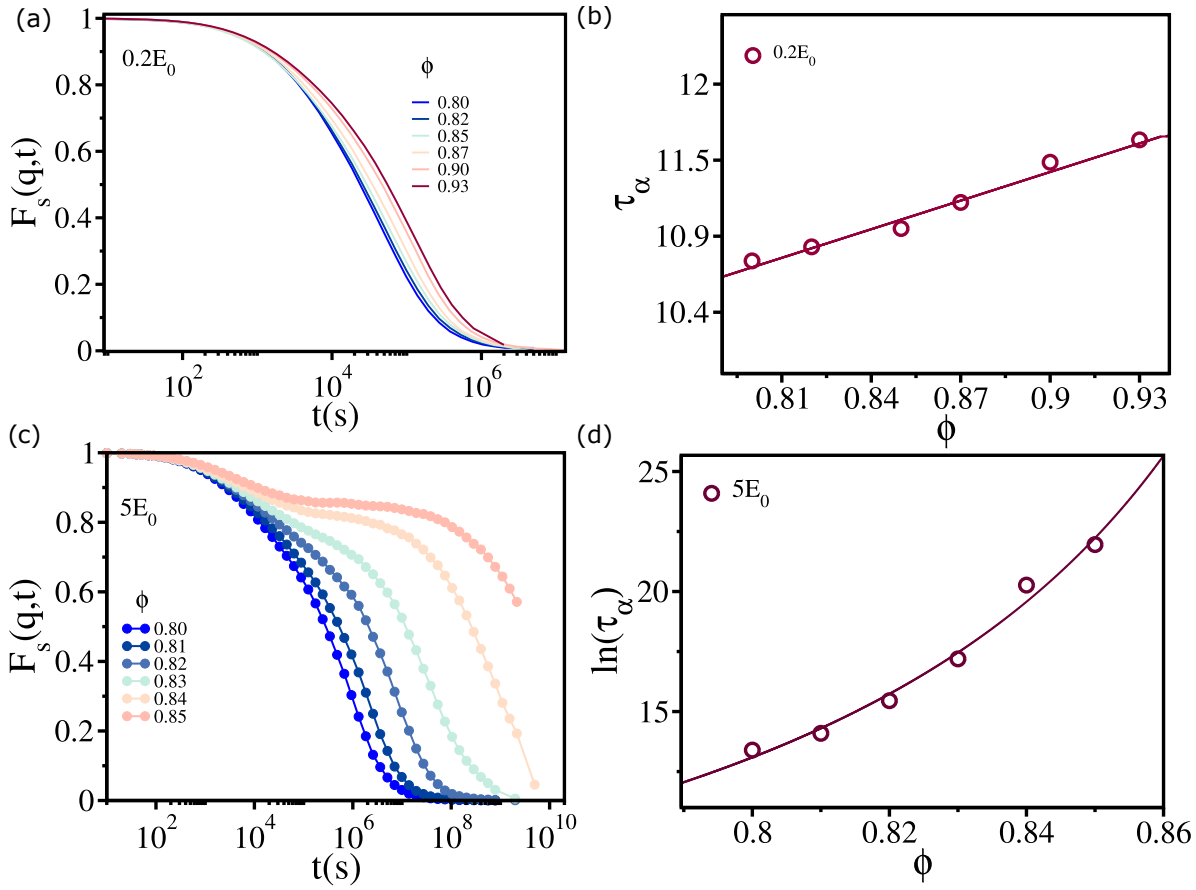

FIG. S11: *Liquid and glass states in 2D tissues:* (a) $F_s(q,t)$ as a function of t for various values of ϕ with $E = 0.2E_0$ and $\Sigma = 24.8\%$. (b) Relaxation time, τ_α, as a function of ϕ for $E = 0.2E_0$ and $\Sigma = 24.8\%$. The solid line is fit to $\tau_\alpha = \tau_0 \exp(A\phi)$. (c) Same as (a) except it is for $E = 5E_0$. (d) Same as (b) but for $E = 5E_0$. The solid line is the VFT fit (see Eqn. (2)).

the the protocol used in the glass transition literature, we define ϕ_g in our system as the ϕ where $\tau_\alpha \simeq 10^{11}$. For reference, the glass transition packing fraction $\phi_g \sim 0.58 - 0.60$ [10] for pure hard-sphere liquids. On the other hand for soft tissues, it can occur at a much higher packing fractions [11, 12].

Taken together, the results in presented in this section show that all the phases and dynamical behavior found in 3D are recapitulated in 2D as well.

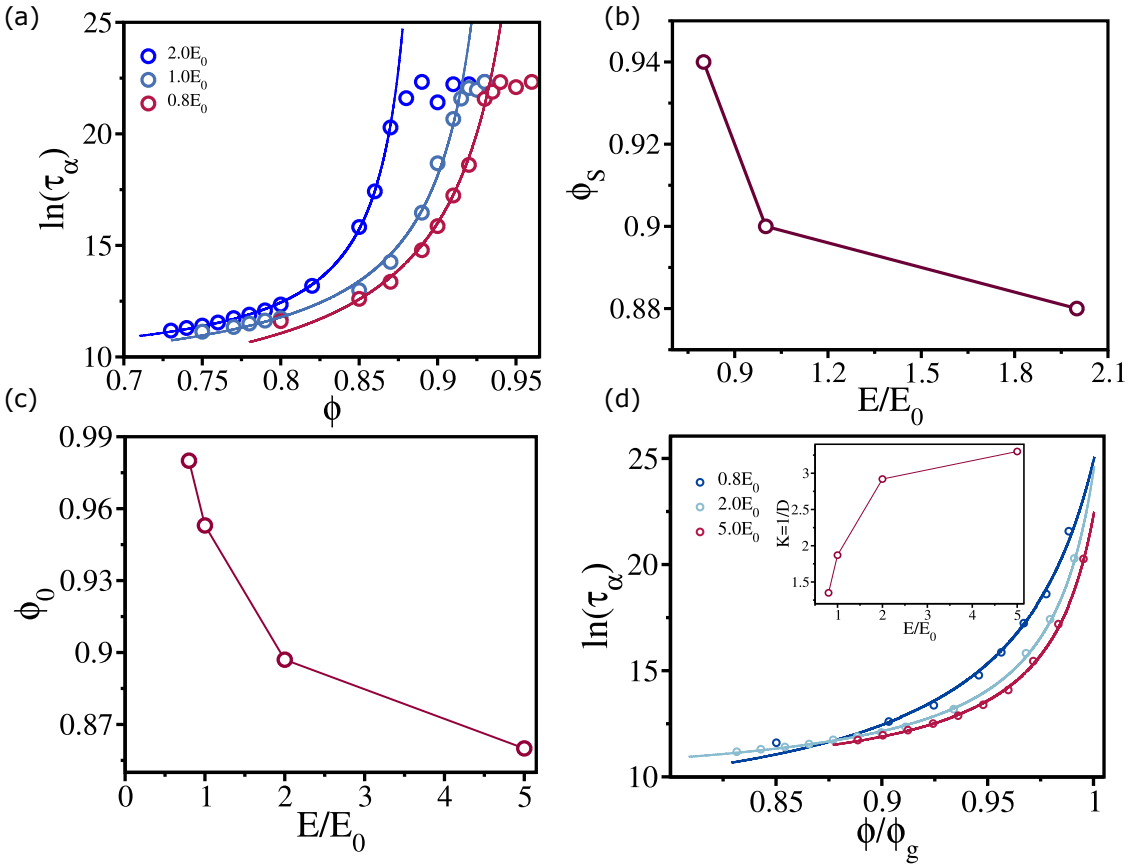

FIG. S12: *Saturation of τ_α in 2D tissues:* (a) τ_α as a function of ϕ for $E = 0.8E_0, 1.0E_0$ and $2.0E_0$ with $\Sigma = 24.8\%$. The solid lines are fit to the equation (2). (b) The critical packing fraction ϕ_S above which τ_α saturates, as a function of E. (c) ϕ_0 as a function of E. (d) $\ln(\tau_\alpha)$ as a function of ϕ/ϕ_g. Inset shows kinetic fragility $K_{VFT} = 1/D$ as a function of E/E_0. Here $\Sigma = 24.8\%$.

X. SIMULATION PARAMETERS

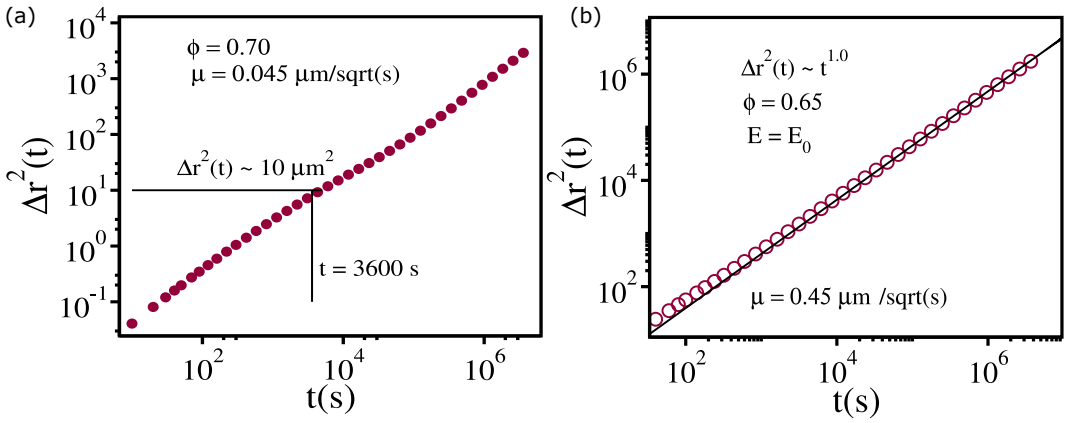

FIG. S13: *Importance of self-propulsion:* (a) MSD $\Delta r^2(t)$ as a function of t at $\phi = 0.70$ in 2D with $E = E_0$, $\Sigma = 8.5\%$, $\mu = 0.045\mu m/\sqrt{s}$. (b) Same as (b) but for 3D with $E = E_0$, $\mu = 0.45\mu m/\sqrt{s}$, $\Sigma = 8.5\%$ at $\phi = 0.65$.

TABLE I: Parameters used in the simulations.

Parameters	**Values**	**References**
Timestep (Δt)	10s	[2]
Self-propulsion (μ)	0.045 μm/$\sqrt{\text{s}}$	[2]
Friction coefficient (γ_o)	0.1 kg/(μm s)	[2]
Mean Cell Elastic Modulus (E_i)	$0.1E_0$ – $8.0E_0$	[13, 14]
Mean Cell Poisson Ratio (ν_i)	0.5	[14, 15]

[1] Zane Shi, Pablo G. Debenedetti, and Frank H. Stillinger. Relaxation processes in liquids: Variations on a theme by Stokes and Einstein. *The Journal of Chemical Physics*, 138(12):12A526, 01 2013.

[2] Rajsekhar Das, Sumit Sinha, Xin Li, T. R. Kirkpatrick, and D. Thirumalai. Free volume theory explains the unusual behavior of viscosity in a non-confluent tissue during morphogenesis.

eLife, 12:RP87966, 2024.

[3] Morrel H. Cohen and David Turnbull. Molecular transport in liquids and glasses. *The Journal of Chemical Physics*, 31(5):1164–1169, 1959.

[4] David Turnbull and Morrel H. Cohen. Free-volume model of the amorphous phase: Glass transition. *The Journal of Chemical Physics*, 34(1):120–125, 1961.

[5] David Turnbull and Morrel H. Cohen. On the free-volume model of the liquid-glass transition. *The Journal of Chemical Physics*, 52(6):3038–3041, 1970.

[6] Kerstin Falk, Daniele Savio, and Michael Moseler. Nonempirical free volume viscosity model for alkane lubricants under severe pressures. *Physical Review Letters*, 124:105501, 2020.

[7] Nicoletta I. Petridou, Bernat Corominas-Murtra, Carl-Philipp Heisenberg, and Edouard Hannezo. Rigidity percolation uncovers a structural basis for embryonic tissue phase transitions. *Cell*, 184(7):1914–1928.e19, 2021.

[8] Daniel Faken and Hannes Jónsson. Systematic analysis of local atomic structure combined with 3d computer graphics. *Computational Materials Science*, 2(2):279–286, Mar 1994.

[9] Alexander Stukowski. Structure identification methods for atomistic simulations of crystalline materials. *Modelling and Simulation in Materials Science and Engineering*, 20(4):045021, May 2012.

[10] W. van Megen and S. M. Underwood. Glass transition in colloidal hard spheres: Measurement and mode-coupling-theory analysis of the coherent intermediate scattering function. *Phys. Rev. E*, 49:4206–4220, 1994.

[11] Thomas E. Angelini, Edouard Hannezo, Xavier Trepat, Manuel Marquez, Jeffrey J. Fredberg, and David A. Weitz. Glass-like dynamics of collective cell migration. *Proceedings of the National Academy of Sciences*, 108(12):4714–4719, 2011.

[12] Dapeng Bi, J. H. Lopez, J. M. Schwarz, and M. Lisa Manning. A density-independent rigidity transition in biological tissues. *Nature Physics*, 11(12):1074–1079, 2015.

[13] Jörg Galle, Markus Loeffler, and Dirk Drasdo. Modeling the effect of deregulated proliferation and apoptosis on the growth dynamics of epithelial cell populations in vitro. *Biophysical Journal*, 88(1):62–75, 2005.

[14] Abdul N Malmi-Kakkada, Xin Li, Himadri S Samanta, Sumit Sinha, and Dave Thirumalai. Cell growth rate dictates the onset of glass to fluidlike transition and long time superdiffusion in an evolving cell colony. *Physical Review X*, 8(2):021025, 2018.

[15] Gernot Schaller and Michael Meyer-Hermann. Multicellular tumor spheroid in an off-lattice voronoi-delaunay cell model. *Physical Review E*, 71(5):051910, 2005.